THE POTENTIAL OF SMARTLNB NETWORKS FOR RAINFALL ESTIMATION

Filippo Giannetti[1], Marco Moretti[1], Ruggero Reggiannini[1], Antonio Petrolino[2], Giacomo Bacci[2], Elisa Adirosi[3], Luca Baldini[3], Luca Facheris[3], Samantha Melani[4], Alberto Ortolani[4]

[1] University of Pisa, Pisa, Italy, [2] MBI S.r.l., Pisa, Italy, [3] CNIT-Laboratorio Nazionale di Radar e Sistemi di Sorveglianza, Pisa, Italy, [4] CNR IBIMET, Florence, Italy

ABSTRACT

NEFOCAST is a research project that aims at retrieving rainfall fields from channel attenuation measurements on satellite links. Rainfall estimation algorithms rely on the deviation of the measured E_s/N_0 from the clear-sky conditions. Unfortunately, clear-sky measurements exhibit signal fluctuations (due to a variety of causes) which could generate false rain detections and reduce estimation accuracy. In this paper we first review the main causes of random amplitude fluctuations in the received E_s/N_0, and then we present an adaptive tracking algorithm based on two Kalman filters: one that tracks slow changes in E_s/N_0 due to external causes and another which tracks fast E_s/N_0 variations due to rain. A comparison of the outputs of the two filters confirms the reliability of the rainfall rate estimate.

Index Terms— Rain attenuation in satellite links; Kalman filter; rain fields evaluation; nowcasting.

1. INTRODUCTION

Traditional systems for rainfall measurement use telemetered rain gauges, weather radars and or satellite-borne sensors. Rain gauges provide accurate sparse pointwise measurements of rainfall accumulation, but reconstructing precipitation fields requires using interpolation techniques. A weather radar provides seamless measurements of precipitations with high spatial resolution, but its estimates are affected by many error sources (calibration, ground clutter, partial beam blocking, propagation effects precipitation attenuation, etc.). Furthermore, at far distance the broadening of the radar beam and the increase of the beam height respect to ground worsens the spatial resolution and the accuracy of the estimate of precipitation at ground level [1]. Satellite precipitation observations can provide measurements over areas where ground instrumentation is not available, but have a coarse space and time resolution. In opposition to the systems described above, "signals of opportunity", i.e., terrestrial or satellite microwave links, can be used. This is the case of the NEFOCAST project (originally named SVI.I.C.T.PRECIP,), funded by the Tuscany Region, Italy. Actually, NEFOCAST uses a dense population of interactive satellite terminals (ISTs) that serve as both weather sensors and modems to send the measurements to a dedicated nowcasting platform and to receive back rainfall information and potential alerts. The IST used for the project is an innovative EUTELSAT's product named SmartLNB (smart low-noise block converter) [2], which shall replace the traditional satellite receivers, providing at the same time additional interactive services through a low rate return channel. Figure 1 illustrates NEFOCAST architecture for real-time and wide-area rain-rate estimations. The estimates of the rain rate are obtained from SmartLNB's measurements of satellite signal attenuation, and thus have quasi-instantaneous nature, whereas the rain gauge measurement represents a cumulated value over a certain interval. Observations from both the SmartLNBs and the tipping bucket rain gauge sensors, as the reference benchmark, are sent to a satellite hub. The NEFOCAST service center collects both SmartLNB and rain gauge data from the satellite and generates rain field maps that are shared with value-added service providers (VASPs).

2. THE SMARTLNB DEVICE AS A RAIN GAUGE

The SmartLNBs receive the forward link (FL) signal from EUTELSAT 10A geostationary satellite (Tab. 1) in DVB-S2 format, with EIRP=48 dBW, mod-cod QPSK 4/5, frequency 11345.8 MHz and vertical linear polarization (VLP). Power level measurements carried by the SmartLNBs are periodically collected by the NEFOCAST service center via the return link (RL), using the asynchronous F-SIM protocol [3], with frequency 14216.6 MHz and linear horizontal polarization (LHP). Figure 2 illustrates the geometry used for rainfall estimation under the simplified hypothesis of a stratiform precipitation, with a clear separation, at height h_0, between a layer of ice above the 0° isothermal and the melting layer (whose bottom is at height h_r). Knowing the total attenuation (from SmartLNB measures) and the path length (from geometry), the specific attenuation is evaluated and rain rate is estimated using a special relationship. Figure 3 demonstrates that rainfall rate estimate of a SmartLNB is in a good agreement with that provided by a nearby rain gauge. NEFOCAST provides a sort of average along the path, whereas the rain gauge measures the rain accumulation, a perfect matching between the two estimates is impossible.

Table 1. Summary of satellite link main parameters

Feature / Item	Name / Value /
Satellite	Eutelsat 10A, 10º East
RL frequency & polarization	14.216 GHz, LHP
FL frequency & polarization	11.345 GHz, LVP
FL protocol, RL protocol	DVB-S2, F-SIM

3. SETTING A RELIABLE REFERENCE LEVEL

Even in clear-sky, the received signal from a satellite is affected by many impairments that cause amplitude fluctuations, as shown in the recording plotted in Fig. 4.

3.1. Scintillation fading

Scintillation fading denotes rapid fluctuations in signal amplitude (inset box of Fig. 4) caused by small-scale irregularities in the tropospheric refractive index. This effect is appreciable for frequencies above 10 GHz and grows with increasing frequency [4]. In K_u band, fluctuations are within ±0.5 dB [5]. In the gigahertz frequency range, the period of scintillation fades varies from 1 to 10 sec. [6] and, accordingly, the spectral width of the fluctuations in the K_u band is about 0.1 Hz [5]. These fluctuations are thus much faster than the rain events and even faster if compared to the long-term effects mentioned in Sects. 3.2-3.3 and as such can be smoothed out by a Kalman filter (Sect. 4).

3.2. Orbit perturbations

In practice, a satellite is subject to many sources of perturbations that make impossible to maintain its orbit perfectly stable. One of the main orbit perturbations is related to the gravitational effects of the moon and the sun that cause a progression of the orbit inclination [7]. Perturbations are periodically counteracted by means orbit correction manoeuvers. The residual orbit inclination causes an apparent daily movement of the satellite in elevation and longitude, as seen from the ground station, along an 8-shaped path, with a 24-h period. The value of the receiving antenna gain towards the satellite is thus continuously changing and causes the 24-h periodic fluctuations in Fig. 4. These long-term signal fluctuations can be effectively tracked using a sufficiently slow Kalman filter (Sect. 4).

3.3. Other sources of long-term signal fluctuations

Further slow variations of the received signal amplitude are caused by drift of satellite's orbital position [7] or by beam-bending caused by large-scale changes in refractive index changes [8], due to the atmosphere's temperature and humidity variations. However, both of them have slow dynamics and can be tracked by the same Kalman filter (Sect. 4).
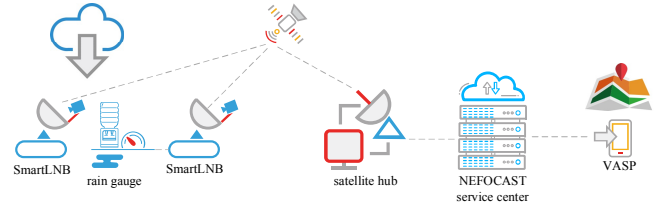
Fig. 1. NEFOCAST experimentation network for real-time wide-area high-spatial resolution rain-rate measurement.
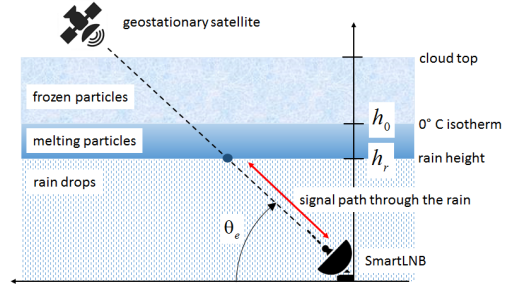
Fig. 2. Downlink geometry with stratiform rain.
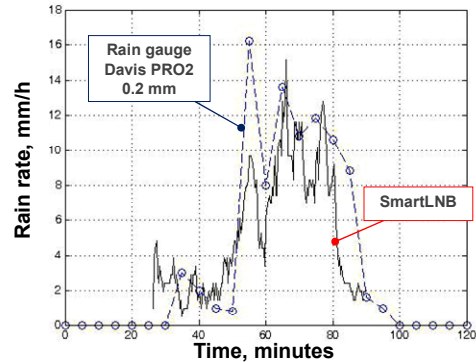
Fig. 3. Rain rate estimate obtained from SmartLNB measurements compared with rain gauge measurements.

3.4. Sun transit

Around the equinoxes, the Earth receiving stations aimed at a geostationary satellite are occasionally "blinded" by the sun's apparent passage behind the satellite. This phenomenon, which is referred to as sun transit, lasts a few minutes daily, over a period of a few days. During the transit, the sun's noise heavily interferes with the satellite's FL signal. This leads to an increase of the antenna noise temperature and causes deep fades of the ratio E_s/N_0 between the average radiofrequency received energy within the time interval of one information-bearing symbol (E_s) and the one-sided power spectral density of the channel's Gaussian noise (N_0) (Fig. 4) [9]. However the date, the time and the duration of any sun transit can be accurately predicted, and therefore, such

an issue could be effectively tackled with a proper management of the SmartLNB measurements. For instance, the last measured value of E_s/N_0 prior to sun transit could be kept fixed for the whole duration of the fade event.
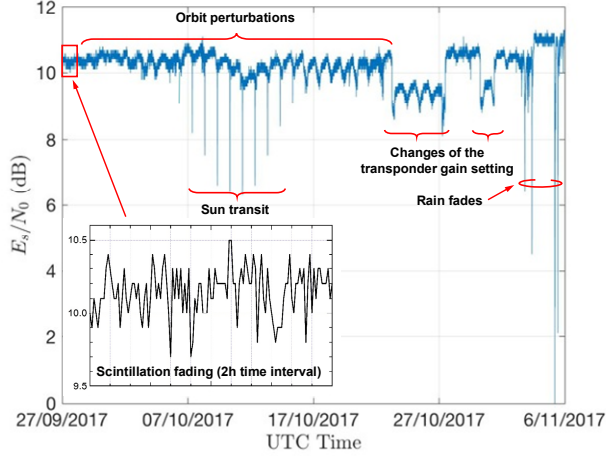

Fig. 4. Sample of E_s/N_0 measurements with several sources of reference level impairments.

3.5. Changes of the transponder gain setting

Occasionally, the satellite operator changes the transponder gain setting due to customer requests or other operational needs. If the change consists in a power reduction (as in Fig. 4), the analysis of the real-time data provided by the SmartLNBs will misinterpret it as the onset of a precipitative event. However, such an artificial signal fade simultaneously affects in the same manner the data from all the active sensors, and therefore it can be easily detected and ignored by a global management of the data at the processing center.
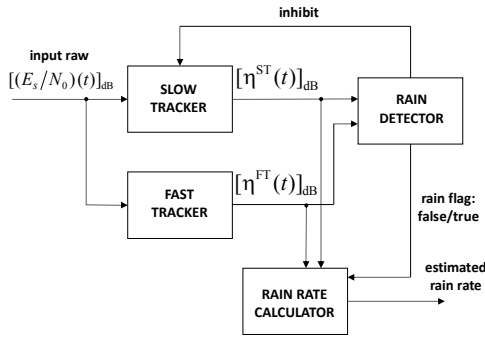

Fig. 5. Architecture of the double Kalman filter.

4. DOUBLE KALMAN TRACKING

Due to the concurrent impact of the phenomena outlined in Sects. 3.1-3.5, the values of $[(E_s/N_0)(t)]_{dB}$ measured in clear-sky conditions are far from being constant and undergo sig-

nificant fluctuations, whose peak-to-peak deviations may easily sum up to 1 dB or more (Fig. 4). The clear-sky signal level variance prevents the estimation of the rain rate using a *fixed* threshold $[E_s/N_0]_{dB}^{(ClearSky)}$, against which to evaluate rain attenuation. Rather, it seems reasonable to use a time-variable reference matching the slow variations due to station-keeping (Sect. 3.2) and, at the same time, being as insensitive as possible to faster disturbances. The solution pursued here is based on the use of a 2-state Kalman filter (*slow tracker*, ST) [10] with parameters appropriately geared so as to have its output $[\eta^{ST}(t)]_{dB}$ track the above mentioned long-term variations of clear-sky $[(E_s/N_0)(t)]_{dB}$. Furthermore, the filter dynamics must be slow enough to make $[\eta^{ST}(t)]_{dB}$ almost insensitive to changes of $[(E_s/N_0)(t)]_{dB}$ due to the onset of rain events, whose time of occurrence is typically in the order of several minutes. In addition to the above filter, a second Kalman filter (*fast tracker*, FT) has been implemented providing an output $[\eta^{FT}(t)]_{dB}$ which follows the fluctuations of $[(E_s/N_0)(t)]_{dB}$ due to rain, but still capable of smoothing out most of the scintillation noise (details of the filter design cannot be pursued here for space limits). The above approach leads to an architecture employing a double, slow/fast, tracker as sketched in Fig. 5. The underlying idea is as follows: in clear-sky conditions the outputs of the two trackers, both driven by $[(E_s/N_0)(t)]_{dB}$, approximately provide the same filtered output (i.e., $|[\eta^{FT}(t)]_{dB}-[\eta^{ST}(t)]_{dB}| \approx 0.1$ dB) while, at rain onset, the FT output $[\eta^{FT}(t)]_{dB}$ starts following the variation of $[(E_s/N_0)(t)]_{dB}$ due to rain and may deviate significantly (downwards) from $[\eta^{ST}(t)]_{dB}$. Rain is assumed present when the difference between the two outputs $|[\eta^{FT}(t)]_{dB}-[\eta^{ST}(t)]_{dB}|$ exceeds a given detection threshold (here fixed to 0.3 dB). The latter entails a lower limit to the detectable rain rate, which must be traded off against the false rain detection rate. The "rain detector" block detects the crossings of the above threshold and sets a *rain flag*. It also activates a sequence of measures (not discussed here due to lack of space) aimed at making sure that the dip of $[(E_s/N_0)(t)]_{dB}$ is due to actual rain and is not a fake. The "rain rate calculator" evaluates the instantaneous difference (in dB) between the ST and FT outputs and provides an estimate of the average rain rate along the signal path using the following formula:

$$r = \alpha L_{1,dB}^{\beta} \quad [\text{mm/h}], \tag{1}$$

where α and β are coefficients depending on frequency and on the climatic zone of the receiver location [11], and $L_{1,dB}$ is the specific rain attenuation (in dB/km), given by

$$L_{1,dB} = L_{dB} \sin \theta_e / h_r. \tag{2}$$

Here h_r and θ_e denote the rain height (km), taken as the bottom of the melting layer, and the elevation angle of the antenna, respectively, and $L_{dB} = 10 \log L$ is the overall attenuation (dB) undergone by the received signal along the path through the rain, from the clouds to the ground terminal, with L given by:

$$L(t) = \frac{\left[\dfrac{\eta^{ST}(t)}{\eta^{FT}(t)}\right]\left[\dfrac{T_{C}}{L_{A}} + T_{M}\left(1 - \dfrac{1}{L_{A}}\right) + T_{G} + T_{R}\right] + \dfrac{T_{M} - T_{C}}{L_{A}}}{T_{M} + T_{G} + T_{R}} \quad , \quad (3)$$

where L_{A} is the atmospheric attenuation and the noise temperatures of cosmos, meteorological formations, ground and receiver hardware are $T_{C} \simeq 3$ K , $T_{M} \simeq 275$ K , $T_{G} \simeq 50$ K and $T_{R} \simeq 14$ K , respectively [7]. During a rain event, the rain flag is set to *true* and the ST state is "frozen" in the condition it was in when the rain started. This choice could lead to the accumulation of errors in case of long rain events (a few hours), but very often it is acceptable because precipitation is typically an intermittent phenomenon even when it is very intense on the average. At the end of the rain event, the FT state returns in the close proximity of the ST state, and when the difference between the outputs of the two trackers falls below a further threshold (e.g., 0.1 dB), the rain detector states "end of rain" and resets the flag to *false*. As an example, the upper part of Fig. 6 shows the raw $[(E_{s}/N_{0})(t)]_{dB}$ (light blue line) and the outputs of the two trackers (black: $[\eta^{ST}(t)]_{dB}$; red: $[\eta^{FT}(t)]_{dB}$). Results show that in the absence of rain the outputs of the two filters are almost coincident, while during the precipitation event they depart significantly from one another. Using (1)-(3) the rain rate is calculated, and the result is shown in the bottom of Fig. 6.

5. DATA PROCESSING FOR RAIN FIELD ESTIMATION

On-ground 2D rain rate fields are obtained by collecting the attenuation measurements from the SmartLNBs and by using a 2-step procedure which generates real-time maps of rain distribution at ground. First, the value of the specific signal attenuation is evaluated using (3) and (2) at the sites of the SmartLNBs (Sect. 4). To this end, in addition to the attenuation measurements, it is necessary at least the knowledge of the maximum height of precipitation h_{r} which is estimated from the altitude of the 0° C isotherm h_{0}. The latter is derived from atmospheric simulations performed using a meteorological model, such as the WRF-ARW model. The second step consists in determining the 2D field of the ground rain rate. A first implementation is based on a simple spatialisation of the measurements of the rain rate obtained in the previous step. A more complex approach is currently under development in order to introduce the information related to the spatial and temporal correlations of the precipitating phenomena under investigation. The idea is to propagate such information through a Kalman filter, after estimating both the spatial kinetics and the intensity dynamic of the phenomenon. The rain field maps will be eventually made available to service integrators through a public API. It will then be possible to show them in end-user applications or integrate them in other systems (e.g. weather forecast, logistics, etc.).
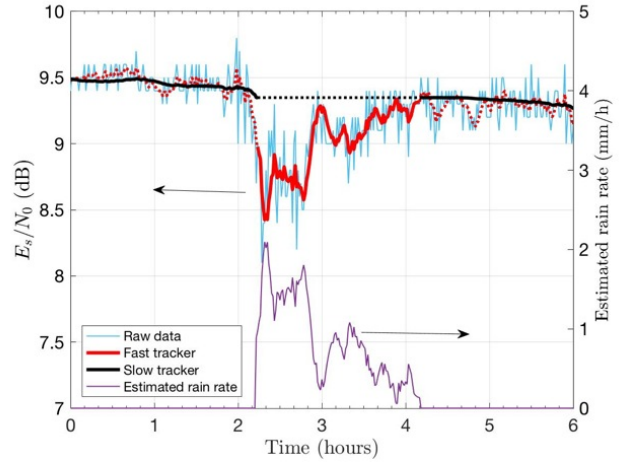

Fig. 6. Smoothing and tracking of the acquired E_{s}/N_{0} using a double Kalman filter in the presence of a rain event.

6. CONCLUSIONS

In this paper we have presented an algorithm based on Kalman filtering to estimate rainfall precipitation on the base of satellite links channel attenuation measurements. The proposed 2-filter architecture employs a mode for slowly tracking the reference-value in clear-sky conditions and a mode for tracking channel attenuation during rain bursts. In spite of the several impairments that cause random amplitude fluctuations of the received E_{s}/N_{0}, experimental results have shown that the proposed solution is very promising for accurate rainfall rate estimation.

7. ACKNOWLEDGMENTS

8. REFERENCES

[1] S. Sebastianelli *et al.*, *"On precipitation measurements collected by a weather radar and a rain gauge network,"* Nat. Hazards Earth Syst. Sci., 13, 605-623, 2013.

[2] Eutelsat SA, SmartLNB website. [Online]. Available: www. eutelsat.com/en/services/broadcast/direct-to-home/ SmartLNB.html (last accessed January 15, 2018).

[3] A. Arcidiacono *et al.*, *"From S-band mobile interactive multimedia to fixed satellite interactive multimedia: making satellite interactivity affordable at Ku-band and Ka-band,"* International Journal of Satellite Communications and Networking ,Vol. 34, Issue 4, July/August 2016, pp. 575–601.

[4] *"Propagation data required for the design of broadcasting-satellite systems,"* Recommendation ITU-R P.679-4, 2005.

[5] M.S.J. Singh, S.I.S. Hassan, M.F. Ain, K. Igarashi, K. Tanaka, and M. Iida, *"Analysis of Tropospheric Scintillation Intensity on Earth to Space in Malaysia,"* American Journal of Applied Sciences 3 (9), pp. 2029-2032, 2006.

[6] R.L. Freeman, *Radio System Design for Telecommunications*, 3rd ed., Wiley Interscience, Hoboken, NJ, 2007.

[7] G. Maral and M. Bousquet, *Satellite Communications Systems*, 5th ed., Wiley, Chichester, UK; 2009.

[8] *"Propagation data and prediction methods required for the design of Earth-space telecommunication systems,"* Recommendation ITU-R P.618-13, 2017.

[9] J. Vankka, A. Kestilä, *"Sun Outage Calculator for Geostationary Orbit Satellites,"* Jurnal Kejuruteraan 26, pp. 21-30, 2014.

[10] Wikipedia, website. [Online]. Available: en.wikipedia.org/wiki/Kalman_filter (last accessed February 1, 2018)

[11] F. Giannetti *et al.*, *"Real-Time Rain Rate Evaluation via Satellite Downlink Signal Attenuation Measurement,"* Sensors, 2017, 17(8).